REPORT DOCUMENTATION PAGE

Form Approved
OMB No. 0704-0188

1. AGENCY USE ONLY *(Leave blank)*	2. REPORT DATE	3. REPORT TYPE AND DATES COVERED
	3-Mar-00	Final Report: 09/06/96 – 12/31/99

4. TITLE AND SUBTITLE

OZONE FLOW TAGGING SCHEME FOR AIR INLET TESTING

5. FUNDING NUMBERS

C: F40600-96-C-0002

6. AUTHOR(S)

PETER A. DEBARBER, PH.D..

7. PERFORMING ORGANIZATION NAME(S) AND ADDRESS(ES)

METROLASER, INC.
18010 SKYPARK CIRCLE #100
IRVINE, CA 92614-6428

8. PERFORMING ORGANIZATION REPORT NO.

TAR9PDF.doc

9. SPONSORING/MONITORING AGENCY NAME(S) AND ADDRESS(ES)

USAF DIRECTORATE OF PROCUREMENT
ARNOLD ENGINEERING DEVELOPMENT CENTER
100 KINDEL DRIVE, SUITE A332
ARNOLD AFB, TN 37389-1332

10. SPONSORING/MONITORING AGENCY REPORT NUMBER

11. SUPPLEMENTARY NOTES

12a. DISTRIBUTION/AVAILABILITY STATEMENT

APPROVED FOR PUBLIC RELEASE; DISTRIBUTION IS UNLIMITED

12b. DISTRIBUTION CODE

A

16. Abstract

Two separately tunable, narrowband excimer lasers were used to photo-dissociate O_2. The O-atom photoproducts rapidly react with ambient O_2 to form O_3, and thus marked a volume of air with a line of ozone. After a fixed time delay, a second laser measured progress of the tagged volume of air by photodissociating ozone, and monitoring the vibrationally excited O_2 photoproduct by planar laser induced fluorescence (PLIF). The spatial displacement of the tagged line was used to measure the velocity in a time-of-flight fashion. Because of ozone's rapid formation (~20 μs) and long chemical lifetime (~2 s), a broad range of velocity measurements are possible.

14. SUBJECT TERMS

Molecular velocimetry, flow tagging, laser diagnostics

15. NUMBER OF PAGES

15

16. PRICE CODE

17. SECURITY CLASSIFICATION OF REPORT	18. SECURITY CLASSIFICATION OF THIS PAGE	19. SECURITY CLASSIFICATION OF ABSTRACT	20. LIMITATION OF ABSTRACT
Unclassified	Unclassified	Unclassified	SAR

NSN 7540-01-280-5500

Standard Form 298 (Rev. 2-89)
Prescribed by ANSI Std. 239-18
298-102

TABLE OF CONTENTS

TABLE OF FIGURES

SUMMARY

The goal of this Phase II work was to develop the prototype core of an ozone tagging velocimetry (OTV) instrument for measuring the structure of velocity flow fields for ground testing of aircraft turbine engines. The proposed innovation was the development of an entirely new molecular flow tagging technique[1] suitable for a wide variety of unseeded flows and application to inlet flows of aircraft turbine engines. The OTV technique requires no seeding of the flow, and is immune from ancillary chemical interferences.

The feasibility of the OTV method was demonstrated in the Phase I program. A broadband ArF excimer laser was used to photo-dissociate O_2. The O-atom photoproducts rapidly react with ambient O_2 to form O_3, and thus marked a volume of air with a line of ozone. After a fixed time delay, a second laser (broadband KrF) measured progress of the tagged volume of air by photodissociating ozone, and monitoring the vibrationally excited O_2 photoproduct by planar laser induced fluorescence (PLIF). The spatial displacement of the tagged line was used to measure the velocity in a time-of-flight fashion. Because of ozone's rapid formation (~20 μs) and long chemical lifetime (~2 s), a broad range of velocity measurements are possible.

In Phase II, the Phase I breadboard concept was expanded into a prototype core appropriate for large-scale facilities. The broadband excimer was replaced with two tunable, narrowband excimer lasers. The new lasers allowed enhanced measurements at higher temporal, spatial, and spectral resolution over larger areas. In Phase II we theoretically and experimentally addressed the operating envelope for applying the OTV method. The remainder of this report discusses the Phase II effort.

INTRODUCTION

The Air Force stated a requirement to measure time-averaged velocity components in air inlets at compressor entrance faces (CEF) for turbine engines.[2] As outlined in the detailed SBIR solicitation from Arnold Engineering Development Center (AEDC), stringent requirements have been placed on the methods sought for such measurement. These requirements included operation in the absence of flow seeding, capability of extensive spatial coverage with high spatial resolution, and non-intrusive probing of the flow. To meet these challenging requirements, a novel laser probe based on an innovative ozone flow tagging technique was investigated and its feasibility demonstrated. This probe represents a significant advancement in measurement technology since, for the first time, velocity measurements can be made directly on unprocessed air without the need for additives (seeding). Since molecular oxygen is a major constituent of atmospheric air, the technique can be readily used in wind tunnels, engine test facilities, shock tunnels, and related aerodynamic test facilities.

Most quantitative laser-based methods for gas flow velocity measurements are based on light scattering from particles seeded into the gas flow. Laser-Doppler Anemometry (LDA) and Particle Imaging Velocimetry (PIV) are two widely used, commercially available methods[3,4]. With the large light-scattering cross-section of particles, particle-based methods can provide very accurate velocity measurements; however, in high-speed flows, the particle seed does not always track the gas velocity. Also, the addition of seeding material into large test flows can be detrimental to the facility. Often, molecular-based velocimetry methods that track the average molecular velocity are preferable.

Molecular-based velocimetry methods have been developed based on measuring the Doppler shift of light scattered from the molecular tracer[5]. In laser-induced fluorescence methods, the Doppler shift of sodium[6], iodine[7], and nitric oxide[8] have been measured to determine the gas flow velocity. The Doppler shift of Rayleigh scattered laser light has been measured with Fabry-Perot interferometers and molecular filters to give the velocity field[9],[10]. Doppler shift methods are often used in high-speed flows but are inaccurate at low velocities where the Doppler shift is extremely small.

Molecular tagging methods are able to track low and high velocities. In these methods, a molecular marker is written into the gas and the velocity is determined by displacement of the marker over time.

Several molecular tagging methods have been developed that rely on seeding of the gas flow. Laser-induced phosphorescence of biacetyl enables the visualization of velocity fields in nitrogen gas flows[11,12]. Since oxygen quenches the phosphorescence of biacetyl, flow tagging measurements using biacetyl are limited to nitrogen flows. Recently, NO grids have been written in gas flows by seeding the flow with NO_2 [13]. Seeded molecular tagging methods are often undesirable. The molecular seed can be toxic or environmentally unfriendly. Furthermore, it is often difficult to generate uniform seeding of the flow.

Several time-of-flight molecular flow tagging velocity measurement techniques have been developed that do not require seeding. The first methods to be developed were based on non-linear optical processes resulting in measurements of limited spatial extent (typically less than 10 mm). In two-photon photodissociation of water vapor (H_2O), a KrF excimer at 248 nm produced a 1.5 mm long marker of the hydroxyl radical (OH) that was subsequently fluoresced to profile flow velocity[14]. In the RELIEF (Raman excitation laser-induced electronic fluorescence) method, a nonlinear stimulated Raman process produces a ~5 mm length of vibrationally-excited oxygen (O_2). The enhanced fluorescence excitation strength of the vibrationally "hot" O_2 over ground state O_2 reveals the displacement of the tag when the flowfield is subsequently irradiated by an ultraviolet (UV) laser[15].

To overcome the problems and limitations of such "non-linear" tagging methods, OTV was developed. The OTV probe utilizes two laser pulses in sequence to first form a tagged molecular species and subsequently to interrogate its displacement after a known time interval. A pulsed ArF excimer laser at 193 nm is used to photodissociate a fraction of the naturally occurring O_2 in the facility airflow. No seeding of the flow is required. This creates O-atom photoproducts that react rapidly with ambient O_2 to form ozone, O_3. As discussed in more detail below, these reactions occur on a timescale far shorter than characteristic flow times, instantaneously "writing" a line of O_3 molecules in the airflow at a set initial time. After a known time delay, which can be adjusted and optimized by the user to match the characteristic flow speeds in a facility, a second, pulsed KrF "interrogation" laser at 248 nm is fired. The output from this laser is configured to produce a sheet that is directed into the flow to intersect the location of the ozone molecules traveling downstream. This interrogation laser serves two purposes: (1) it photodissociates the ozone, forming vibrationally excited O_2 photoproducts extremely rapidly during the short laser pulse, and (2) the pulse is absorbed next by these vibrationally populated O_2 photoproducts which, in turn, fluoresce, identifying the location of the ozone tag. The spatial displacement of the tagged line is used to measure the velocity in a time-of-flight fashion. The OTV approach, represents a major breakthrough in the development of a molecular flow tagging techniques, meeting the stringent requirements for application to unseeded airflows over a wide range of air flow conditions. It is schematically depicted in **Figure 1**.

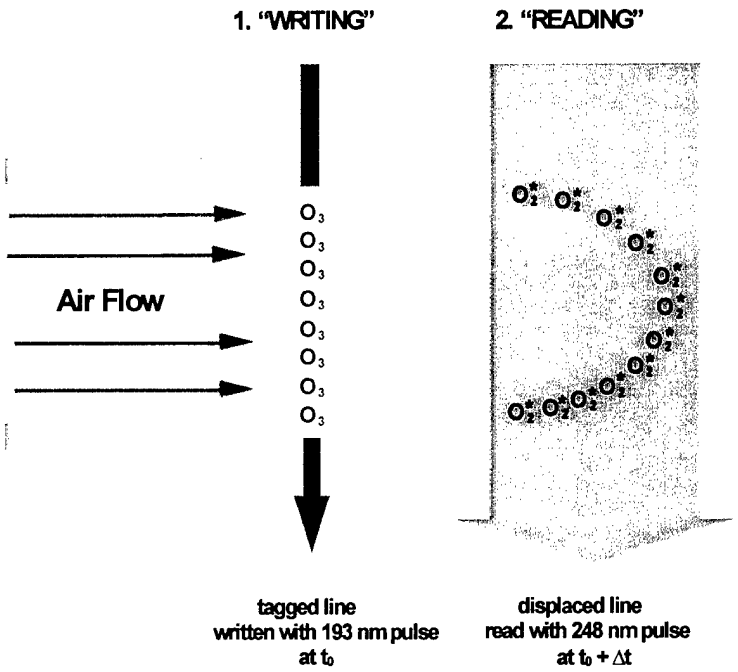

Figure 1. OTV approach schematically represented as two steps: writing and reading.

The Phase II program was structured in three parts: First, an OTV prototype core was assembled and tested in the laboratory at Vanderbilt University. Measurement concepts applicable to AEDC facilities were investigated and the signal characteristics associated with the core system were experimentally measured. Second, the OTV operating envelope was investigated analytically. This was placed in context to the development of the prototype core and the needs of the aeromechanical testing community. Third, the OTV prototype core system was demonstrated to Air Force personnel.

Background Concept and Theory

The OTV velocity measurement relies on two steps: 1) marking the flow initially by "writing" a line of ozone molecules into the flow, and 2) interrogating the flow by "reading" the displacement of the line of ozone as a function of time delay. These two steps are defined by the kinetics and photochemistry of ozone and air. These steps were schematically shown in **Figure 1**, and are discussed in more detail below.

The initial step in the ozone flow tagging scheme is to write a line of ozone molecules in the flow. The absorption of light from an ArF laser at 193 nm by oxygen molecules produces oxygen atoms. The oxygen atoms combine with molecular oxygen to form ozone. This is accomplished through the following sequence of photochemical reactions[16]:

$$O_2 + 193nm \rightarrow 2O(^3P), \qquad k_{prediss} \approx 10^{11}\ s^{-1} \tag{R1}$$

$$O(^3P) + O_2 + M \longrightarrow O_3; \qquad M=N_2, O_2, \qquad k_2=5.7\times10^{-46} m^6 s^{-1}. \tag{R2}$$

Molecular oxygen undergoes efficient predissociation by absorption of ArF radiation in the (4,0) band of the Schumann-Runge continuum. The predissociation rate of reaction R1 is approximately $10^{11} s^{-1}$.[17] Note that the formation of the second $O(^3P)$ atom is actually a quenching of an $O(^1D)$ atom; however this deactivation reaction itself is very fast, and is therefore included in the rate of reaction R1. The formation of ozone is then governed by the three-body reaction rate of R2 which is approximately $5.7\times10^{-46} m^6 s^{-1}$ at a temperature of 300 K for N_2 and O_2 collision partners.[18] The $O(^3P)$ oxygen atoms react with O_2 through a three-body collision mechanism with either N_2 or O_2 to form ozone. The initial position of the tagged line

of ozone molecules is precisely marked by measurement of O_2 Schumann-Runge photofragment fluorescence generated during the pump laser pulse. This emission process is extremely rapid and is ideal as an initial position marker. For the typical tens of milliseconds delay prior to the interrogating laser pulse, the ozone product remains intact as a line of ozone molecules "written" into the flow.

The second step in the ozone flow tagging scheme is to interrogate or "read" the time-of-flight displacement of the tagged ozone line. The optimum mechanism for this step was discovered in the Phase I program. At a set time delay, tailored to the time scale of the particular flow, a 248 nm laser sheet generated from a KrF excimer laser is used to both photodissociate ozone and to effect PLIF of the resulting, vibrationally excited, O_2 photoproduct. The following photochemical reactions outline this second step's process:

$$O_3 + 248nm \longrightarrow O(^3P) + O_2(X^3\Sigma_g^-, v'' \geq 6), \tag{R3}$$

$$O_2(X^3\Sigma_g^-, v''= 6,7) + 248nm \longrightarrow O_2(B^3\Sigma_u^-, v'= 0,1,2), \tag{R4}$$

$$O_2(B^3\Sigma_u^-) \longrightarrow O_2(X^3\Sigma_g^-) + \lambda \geq 248nm. \tag{R5}$$

The resultant emission from the excited molecular oxygen is passed through a UV, long wavelength, pass filter and detected with an intensified CCD camera. The displacement of the fluorescing line of molecular oxygen photoproducts is used to calculate the flow velocity component within the laser sheet as a function of the time delay in a time-of-flight fashion.

Prototype Core

The schematic of the OTV prototype core breadboard is shown in **Figure 2**. The 193 nm output from a narrowband ArF excimer laser (150 mJ/pulse, tunable, 0.003 nm linewidth) is split into two beams that are crossed in the flowfield. The ArF beams are focused to 0.5 mm diameters by 1 m lenses. The total beam travel of the ArF beams is about 2 m leading to loss of about half of the beam energy. The 248 nm output from a narrowband KrF laser (400 mJ/pulse, tunable, 0.001 nm linewidth) is focused by a 1 m cylindrical lens to a sheet 20 mm by 0.5 mm in the flowfield. Light from the flowfield is recorded by Princeton Instrument's intensified charge coupled device (ICCD) camera (576 x 384 pixels) with a f/4.5 Nikkor UV lens. A butyl acetate filter (low pass filter at 255 nm) in front of the camera lens blocks the laser radiation from both UV lasers and records the O_2 fluorescence produced by the KrF read laser.

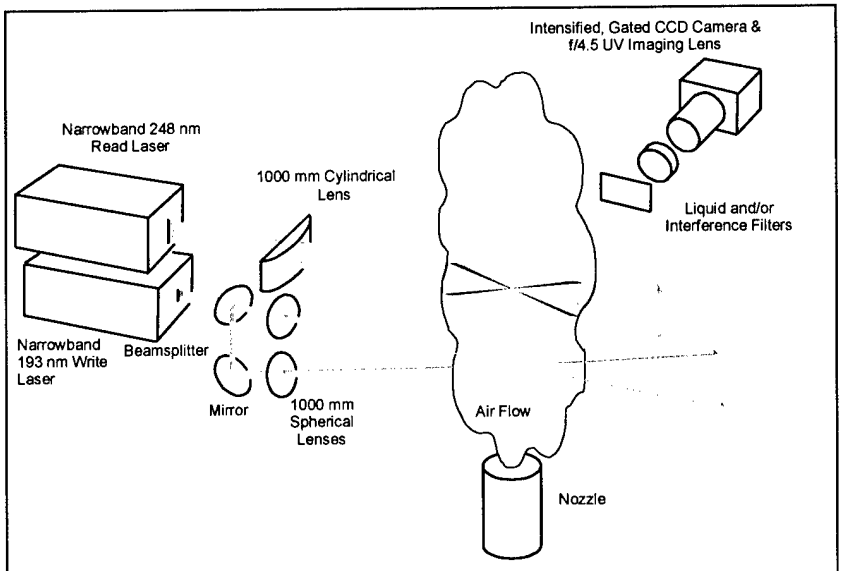

Figure 2. The experimental setup for the OTV prototype core as breadboarded in the laboratory at Vanderbilt University

The presence of vibrationally-excited oxygen for the reading of the tagged line was confirmed by experiment. An excitation scan in room air was used to verify the creation of vibrationally-excited oxygen molecules. To create the ozone, a 50 mJ pulse of 193 nm broadband excimer laser output was focused to a 1 mm beam waist in room air. To probe the photochemically formed ozone, the output from an excimer-

pumped tunable doubled dye laser (~248 nm; 0.8 mJ/pulse) was focused to a 0.5 mm waist. The 248 nm probe radiation was spatially overlapped with the 193 nm pulse. The fluorescence excited by the tunable dye laser as a function of laser wavelength was collected by a Cassegrain mirror system and detected with a photomultiplier tube (PMT). A CCl_4 and UG-11 filter in front of the PMT blocked the 248 nm laser and ambient room light. The 193 nm laser was pulsed and the fluorescence induced by the dye laser fired 1 ms later was measured. The excitation scan is shown in **Figure 3**. The transitions from the Schumann-Runge band are clearly identified, thus showing the presence of vibrationally-excited O_2 photoproduct, $X^2\Sigma_g^-(v''=6,7)$. When the 193 nm beam is blocked, the O_2 transitions completely disappear as expected.

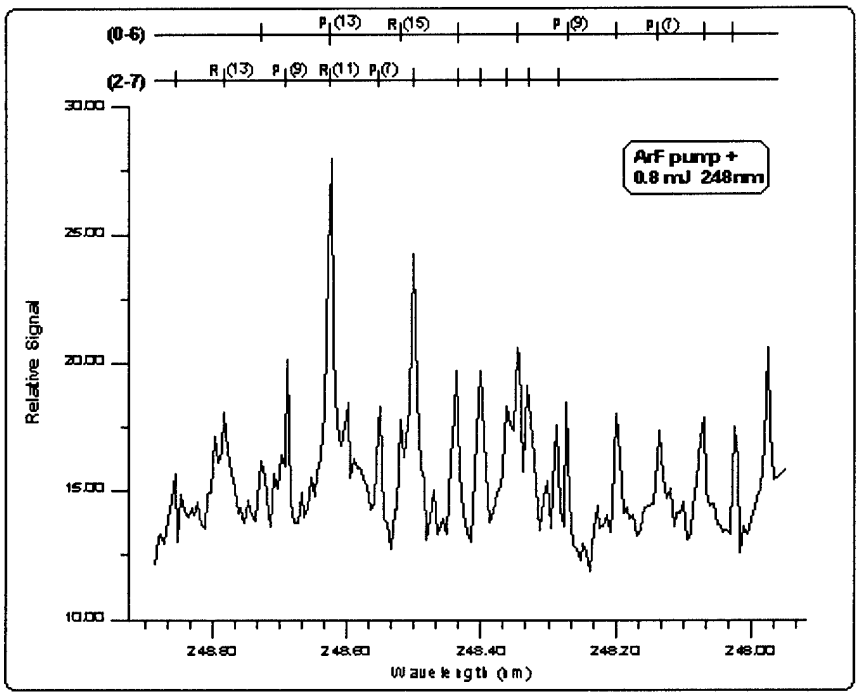

Figure 3. Results showing the fluorescence excitation scan of vibrationally excited O_2 photoproduct.

Operating Envelope

Velocity measurements are needed in a variety of laboratory and test facilities where thermodynamic conditions vary and contaminants are present (e.g., water and nitric oxide). To determine the applicability of the OTV prototype core to airflow velocimetry, chemical kinetics and photochemistry of both ozone and oxygen were carefully examined. The key parameters include reaction rates, laser wavelengths and fluences, pressure, temperature, and chemical composition of the flow environment. The results of this analysis were used to refine design elements of the prototype core.

At the heart of investigation into the operating envelope of the OTV prototype core are chemical kinetics calculations. We analytically investigated the formation rate and destruction rate of ozone for airflow at various temperatures and pressures. In order to predict the concentration of O_3 as a function of temperature, pressure, and time, the CHEMKIN II thermodynamic database and the SENKIN chemical kinetics solver[19] were used with a set of 119 reversible reactions, including reactions involving nitrogen oxides[20].

Ozone concentration levels were calculated as a function of time in three different environments: dry air, humid air (3.5% mole fraction of water at 300 K), and polluted (100 ppm NO) humid air (**Figure 4**). In the case of dry air, the initial mole fractions of N_2, and O_2 are 79.00% and 20.79% respectively. Here it is

assumed that ~1% of the O_2 molecules are photodissociated into O atoms by the ArF laser. About 1% dissociation of the nascent O_2 is expected for typical OTV conditions (10 mJ per 300 μm diameter beam). Here the laser tuned to the P (17) line at 193.293 nm with 0.03 cm^{-1} atm^{-1} absorption[21].

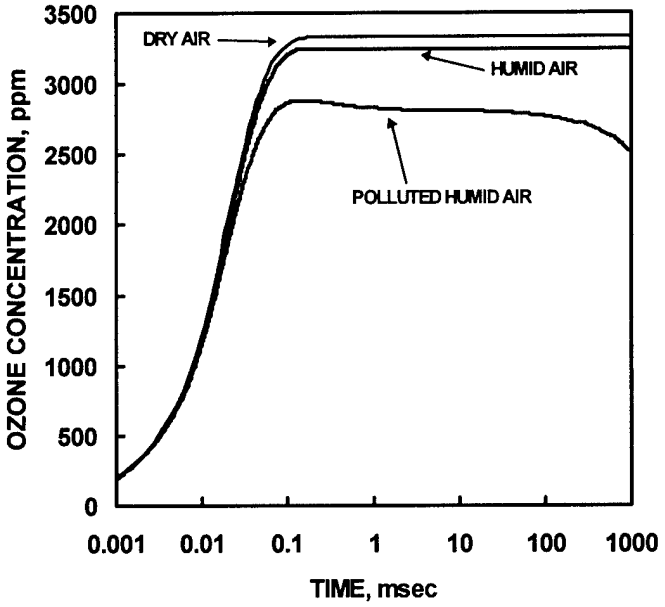

Figure 4. Calculated ozone concentration as a function of time for dry air, humid air, and humid air with 100 ppm of nitric oxide. In all three cases, the temperature was held at 300 K and the pressure was held at 1 atm.

For 1% dissociation of O_2 at 300 K and 1 atm, the estimated initial O atom concentration is 4200 PPM. If all the O atoms formed O_3, one would expect a steady-state concentration of O_3 of 4200 PPM. As seen in **Figure 4**, a slightly lower steady-state O_3 concentration of ~3300 PPM is predicted to occur after ~1 msec. To determine the cause of this ozone deficit, the formation and destruction reactions for ozone were analyzed with the Senkin code. As shown in **Figure 5**, ozone is depleted by the following reaction of ozone with singlet O_2,

$$O_2 (S) + O_3 \rightarrow 2O_2 + O. \qquad (R5)$$

Reaction (R2) controls the O_3 formation as confirmed by its high production rate seen in **Figure 5**. From **Figure 4**, we observe that the O_3 concentration rises rapidly attaining over 50% of its steady-state value within 0.02 ms.

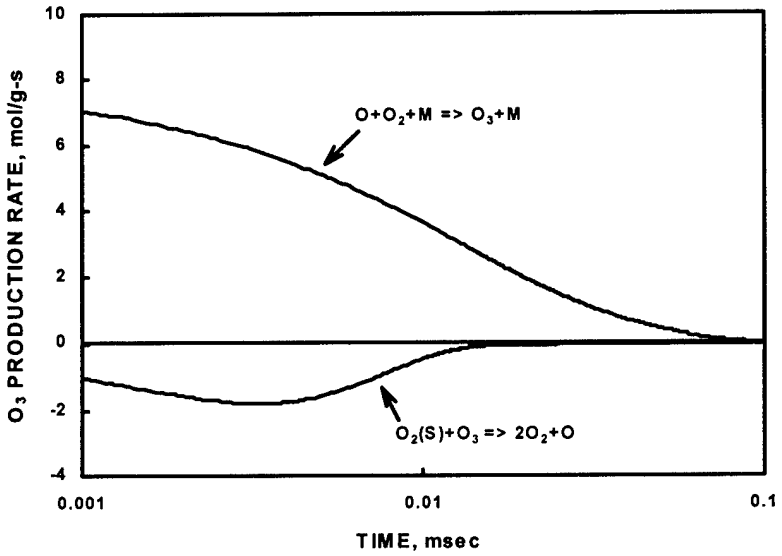

Figure 5. Ozone production rates for humid air with 100 ppm nitric oxide at STP.

In the humid air case, the steady-state O_3 concentrations are lower (**Figure 4**). The slight drop in steady-state O_3 concentration for the humid air is due to an initially lower O_2 concentration (still assuming 1% dissociation of the O_2) and the concomitant lower O atom concentration. The addition of 3.5% mole fraction of water vapor has no appreciable chemical effect on O_3 concentration.

Polluted humid air is modeled with an addition of 100 PPM of NO to the humid air. As seen in **Figure 6**, NO efficiently removes O_3 by following well-known reaction, important in tropospheric pollution modeling[22]:

$$O_3 + NO \rightarrow O_2 + NO_2 . \qquad \text{(R6)}$$

The other two NO reactions shown in **Figure 6** are less important and lead to a slight net production of ozone. We note that a slight temperature rise (~ 30 K) occurs as a result of the initial laser absorption that dissociates O_2 and subsequently releases heat in the formation of O_3 from O and O_2.

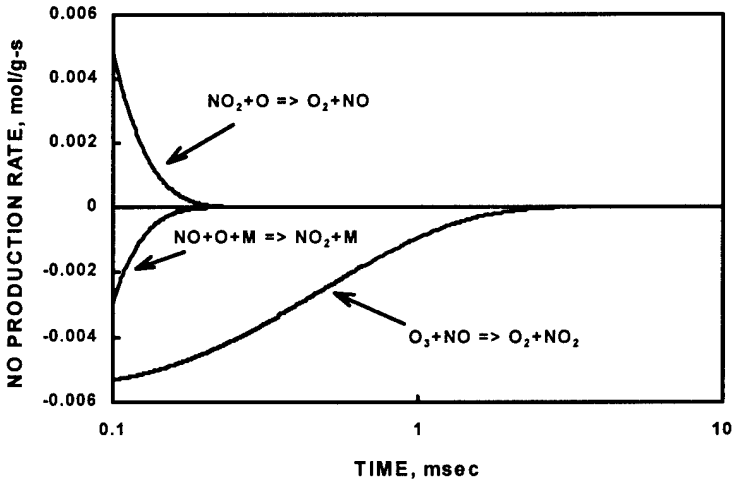

Figure 6. Nitric oxide production rates for humid air with 100 ppm NO at 300 K and 1 atm.

In addition to investigating the effects of the initial chemistry on ozone concentration, we simulated the effects of pressure and temperature on the ozone formation and destruction. These results are summarized in **Figure 7**. At these higher temperatures (500-600 K), the ozone tag persists for about 1 ms; however, higher temperatures have a detrimental effect on the maximum ozone concentration. For atmospheric pressure and 600 K, the maximum ozone concentration is 200 PPM, over 10 times less than the value at 300 K. This drop in peak O_3 concentration is problematic since the read laser produces less fluorescence signal as a result of the lower O_3 and vibrationally-excited O_2 populations. Thus, OTV measurements will be increasingly difficult for temperatures above 600 K.

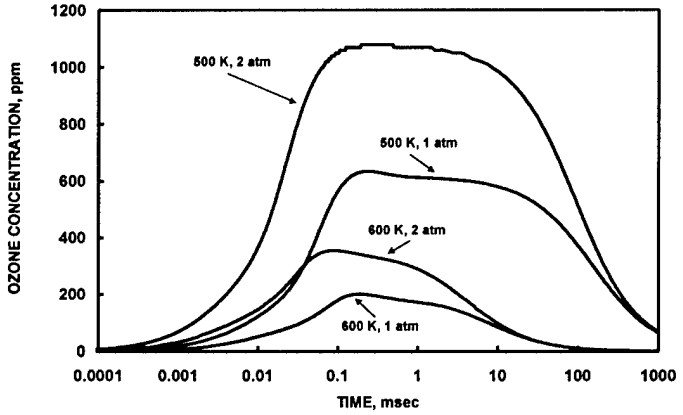

Figure 7. Ozone concentration in dry air for various pressure and temperature conditions.

The important formation and destruction reactions were analyzed for the higher temperature case of 600 K and 1 atm. The major formation reaction remains Reaction (R2). For times less than 0.1 ms, Reaction (R5) is still the major depleting reaction. After about 0.1 ms, two other reactions lead to ozone destruction:

$$O + O_3 \rightarrow O_2 + O_2\,(S) \qquad \text{(R7)}$$

$$O + O_3 \rightarrow 2O_2\,. \qquad \text{(R8)}$$

After about 2 ms, reaction R2 reverses and is the dominant route of ozone destruction. Reactions R5, R7, and R8 also contribute to ozone depletion after 2 ms.

For times less than 2 ms, the O_3 is produced by a thermolecular reaction (R2) while it is destroyed by bimolecular collisions (R5, R8). Since thermolecular reaction rates scale with the square of pressure and bimolecular reactions scale linearly with pressure, the O_3 production rate relative to the destruction rate increases linearly with pressure. As seen in **Figure 7**, doubling the pressure in the simulation leads to about a factor of 2 increase in maximum ozone concentration.

Facility Issues

To determine the applicability of the OTV prototype core to the pressure and temperature conditions of jet engine test facilities, we have superimposed selected conditions of interest for aeromechanical aspects of engine testing onto our results for the ozone number density calculations previously described. In **Figure 8**, contours of constant ozone number density are plotted for various temperature and pressure air inlet conditions. The two static temperature-pressure envelopes correspond to engine inlet Mach numbers of 0.3 and 0.65. The OTV demonstration point corresponds to standard atmospheric conditions typical for our testing at Vanderbilt University. Most aeromechanical test conditions will result in higher concentrations of ozone than the OTV demonstration point. In the worst case, the ozone concentration

will be reduced by about 50% from the OTV demonstration point. Thus, substantial ozone concentrations are expected under the conditions of aeromechanical testing of jet engines.

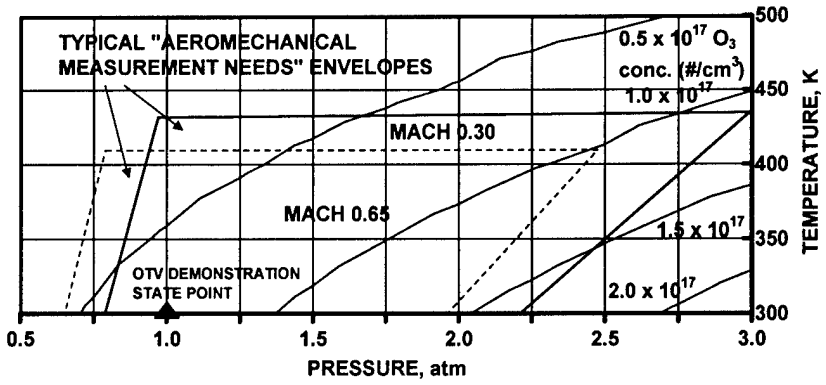

Figure 8. Ozone number density as a function of temperature and pressure for various "aeromechanical" wind tunnel testing conditions.

An important issue in the application of the OTV method to larger scale facility tests is the degree of attenuation of the writing laser beams. At standard temperature and pressure (STP), absorption of the 193 nm laser light by ambient molecular oxygen is a serious concern. An analytical investigation into the optimum wavelength for writing the tagged line was used to arrive at a procedure to minimize beam delivery absorption due to O_2 outside the probe region as a function of propagation distance through ambient air.

Due to the strong attenuation from ambient O_2, especially over large distances, there may be some situations where tuning the laser to line center is not advisable and that a better approach would be to tune off the central absorption maximum. As an illustrative example, we chose to examine laser absorption and ozone signal production in the vicinity of the P(15) line and of position over a 360 cm propagation path. A 360 cm path length is typical of the diameter of a turbine test facility. The P(15) feature was chosen because of its relative strength and proximity to the maximum gain curve for ArF. The feature was modeled with a Lorentzian broadened lineshape of 6.7 cm^{-1} FWHM. The partially resolved doublet lineshape feature is a result of the blended nature of the P(15) line at 51,168.9 cm^{-1} with the adjacent R(17) line at 51,1175.52 cm^{-1} . To arrive at the effective absorptivity that the laser would experience at any given wavelength, the doublet was convoluted with a Gaussian broadened laser lineshape of 0.81 cm^{-1} FWHM, the linewidth of the narrowband ArF excimer laser. Given the absorptivity of oxygen as a function of wavelength, we can estimate the laser intensity for any wavelength at any point along the propagation. This in turn allows us to estimate the ozone produced. The amount of ozone created is directly proportional to the loss of UV intensity over the probe region due to O_2 absorption. For this calculation, a 10 cm long probe region was chosen.

Our analysis estimates the amount of light lost over the following 10 cm probe volume for each frequency and distance from the edge of a test section. In regions close to the edge of the theoretical test section, the highest flux of photons to the probe volume is delivered by tuning to the maximum absorption, (i.e., the center of the P(15) line. As the distance to the probe volume increases, however, the light lost before reaching the probe volume becomes too high and it becomes more advantageous to tune off the maximum absorbance (or tune to a less absorbing feature). When the laser is tuned to the P(15) line center, the point of diminishing returns occurs at roughly 120 cm, which is where αL reaches unity, as shown in **Figure 9.** Here α is the absorption (cm^{-1}) and L is the pathlength (cm). The contour plot of **Figure 10** serves as a guide for laser tuning as a function of path length to the probe volume. The center of the P(15) line is shown at 0 cm^{-1} and the R(17) line is at about 6 cm^{-1}. Our analysis indicates that as propagation distance

increases, tuning the laser off the peak absorption at the line centers of P(15) and R(17) has a beneficial effect.

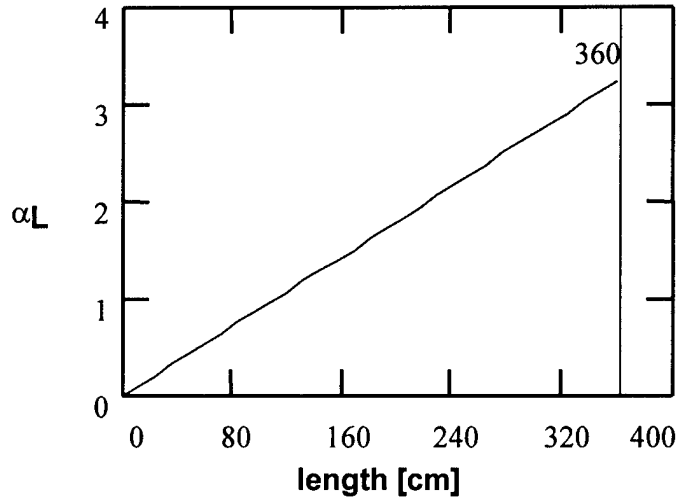

Figure 9. Plot of the product αL vs. the propagation distance L for narrowband absorption at STP conditions.

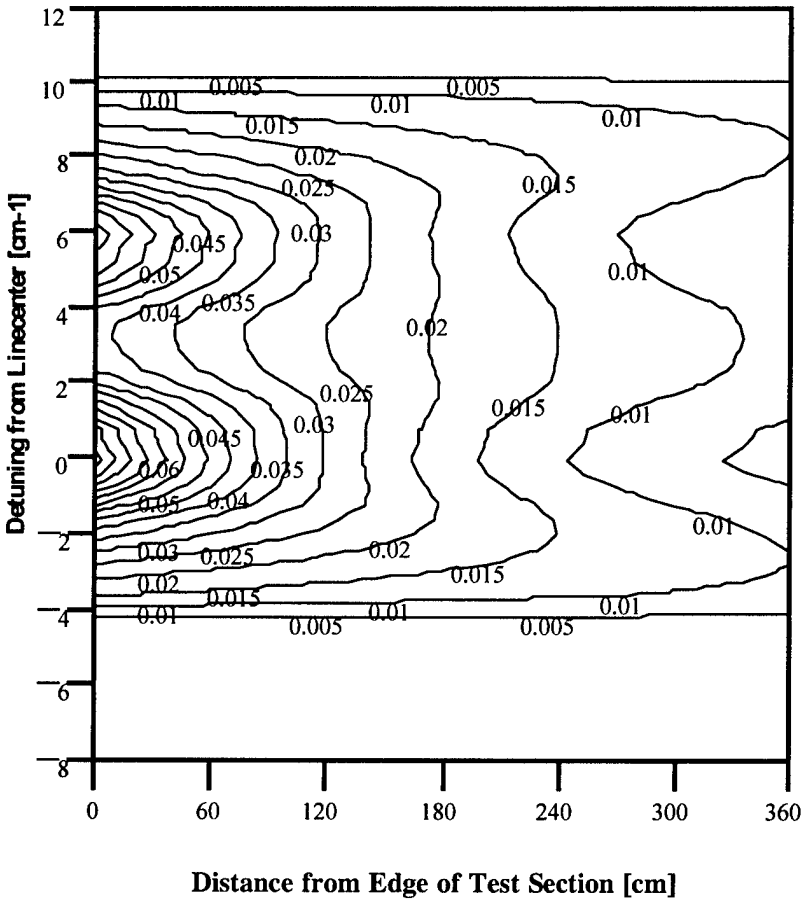

Figure 10. Contour plot of ozone production for a 10 cm probe volume following a beam traverse from the edge of the test section.

Example Data and Analysis

In this section we present two representative examples of OTV data taken with the prototype core in the Vanderbilt University laboratory. The investigations were performed on two different airflow devices: a pulsed speaker-driven nozzle and a Hencken burner nozzle.

Single-shot OTV images of two crossed 193 nm beams were acquired above a 27 mm diameter nozzle. The crossed beam configuration ensured an unambiguous tag marker in space. Air was forced through the nozzle using a large speaker attached to a frequency generator. Modulation of the speaker generated a periodic pulse of air through the nozzle. To generate high–quality, single-shot OTV images, the lasers were both configured to operate narrowband. **Figure 11** is an example of an instantaneous OTV image above the speaker driven airflow through the nozzle. The initial beam crossing pattern (position indicated by the dashed line in the figure) generated with the OTV write laser has been displaced and distorted due to the airflow. The clearly visible vortex structures highlight the flow profiling capability of the OTV method.

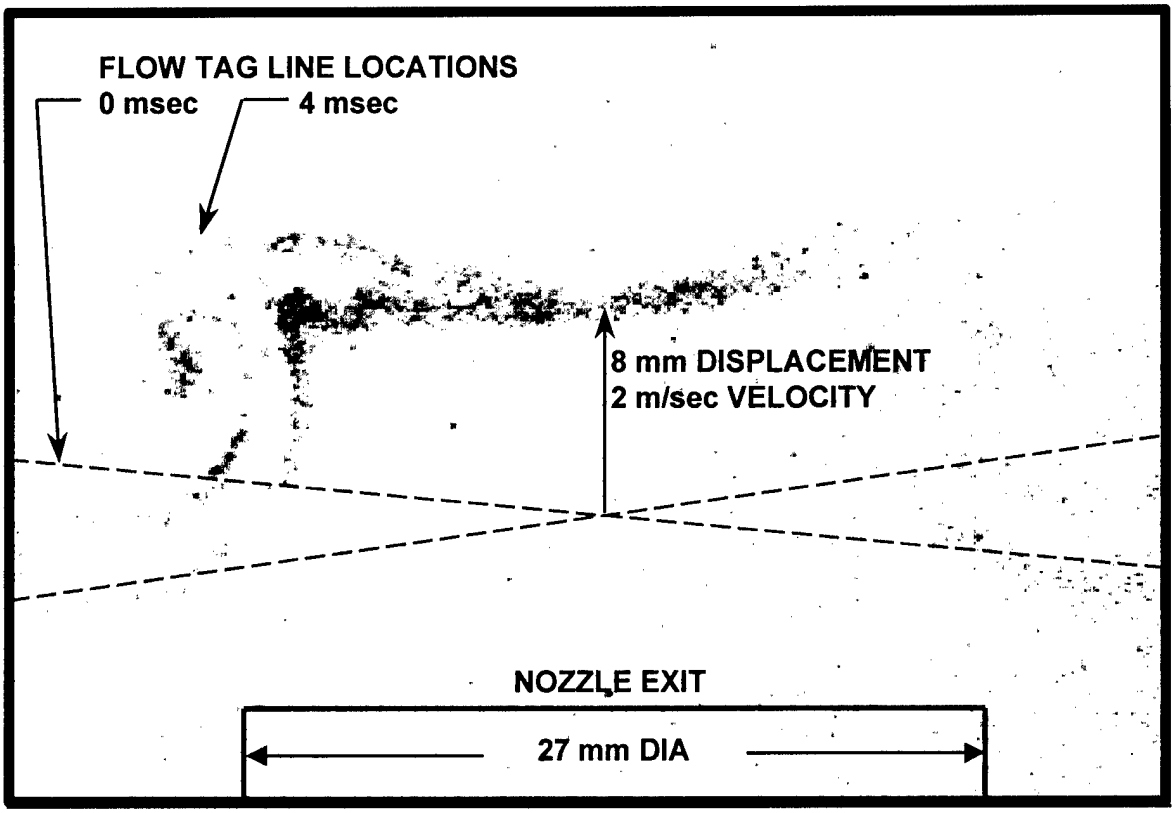

Figure 11. Instantaneous OTV image of vortical flow structure caused by periodically driving air through a 27 mm diameter nozzle attached to a speaker.

To enhance the spatially-resolved mapping capability of the OTV prototype core, we expanded the number of beam crossing points to nine (9) by constructing a 3 x 3 grid of laser beams. This was accomplished by the addition of extra beamsplitters in the paths of the 193 nm writing laser. The resulting pulse energy for each beam defining the grid was on the order of 10 mJ pulse^{-1}. The flow rate was approximately 10 lpm of air through the 12.5 mm diameter Hencken burner. The results of this test are shown in **Figure 12**. This sequence of images shows the average flow direction, and serves to demonstrate the enhanced, spatially resolved, mapping capability of multiple line grid marking of the airflow.

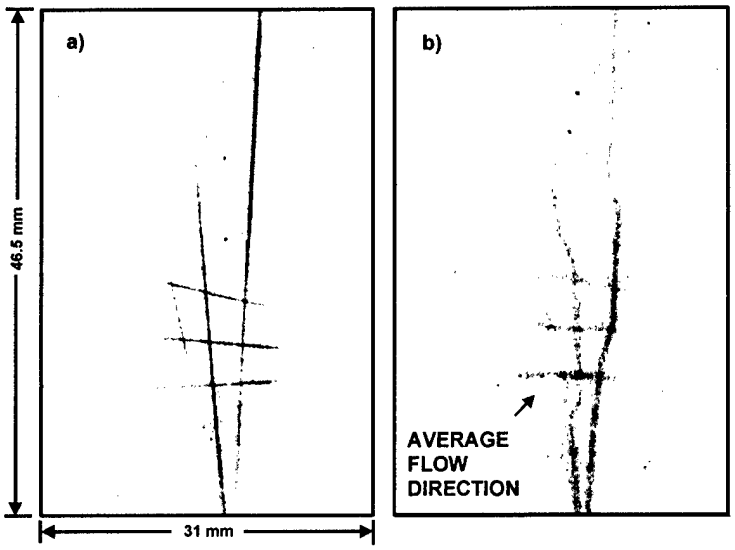

Figure 12. Instantaneous 3 x 3 grid in airflow exiting a 25 mm diameter free jet. (a) No time delay between the write and read pulses. (b) 1 ms time delay between the write and read pulses.

The uncertainty assigned to an OTV measurement is associated with spatial resolution. This uncertainty arises predominantly from two sources: camera resolution and molecular diffusion.

We first consider the uncertainty surrounding camera resolution. The camera we used was a Princeton Instruments 576 ICCD. This camera uses a 576 x 384 pixel array. Each pixel is 22 μm x 22 μm. We binned the camera pixels to 4 x 4 superpixels. Each superpixel images 0.70 mm x 0.70 mm of the flow, and our resolving ability limited the measurement to +/-2 superpixels in a 20 ms measurement interval. Therefore, our camera resolution limited the measurement to 1% accuracy.

We then compared our camera resolution error to the uncertainty associated with molecular diffusional broadening of the line of ozone markers. For this analysis, we considered the measurement of a mean laminar flow velocity by determining the displacement of a volume of laser-generated ozone molecules (OTV) where

$$v = \frac{d}{t}. \tag{1}$$

From established error analysis procedures[23], the uncertainty associated with the velocity measurement is expressed as

$$\Delta v^2 = \Delta d^2 \left(\frac{\partial v}{\partial d}\right)^2 + \Delta t^2 \left(\frac{\partial v}{\partial t}\right)^2. \tag{2}$$

We substitute in the partial derivatives to give

$$\Delta v^2 = \Delta d^2 \frac{1}{t^2} + \Delta t^2 \frac{d^2}{t^4}. \tag{3}$$

For the OTV experiments, $\Delta d/d$ will almost always be much larger than $\Delta t/t$. *A priori*, we know that Δt will be determined by the relative laser jitter and can easily be measured to a precision of $\Delta t \leq 10$ ns. AEDC has specified a target value of $\Delta v/v = 0.01$. Therefore, we can invert Equation (3) to determine our experimentally required value of Δd to satisfy the target velocity measurement accuracy. The caveat here is that measurements can only be made after the marker is formed, *i.e.*, for ozone, $t > 20$ μs.

We find that for $t > 20$ μs (O_3 growth time), the uncertainty in measuring displacement is

$$\Delta d = \sqrt{\Delta v^2 t^2 - \Delta t^2 v^2}, \quad (4)$$

and for $\Delta t = 10$ ns, $t > 20$ μs, and $\Delta v = 0.01 \times v$, we find that the uncertainty in measuring displacement is

$$\Delta d = \sqrt{4 \times 10^{-4}\, t^2 - 1 \times 10^{-16}}\; v. \quad (5)$$

In the absence of turbulence, the marked volume will spread due to diffusion.

For air inlet tests, a temperature range of -60 to 340°F and Mach numbers of M = 0.3 to 0.65 are used[24]. These two ranges determine an operational environment in which 90 m/s ≤ v ≤ 282 m/s. **Figure 13** points out the required accuracy in measuring the displacement for a velocimetry accuracy of 1%. Even over periods of several hundred microseconds, only knowledge of displacement within the diffusion-broadened width is necessary to meet AEDC's requirement.

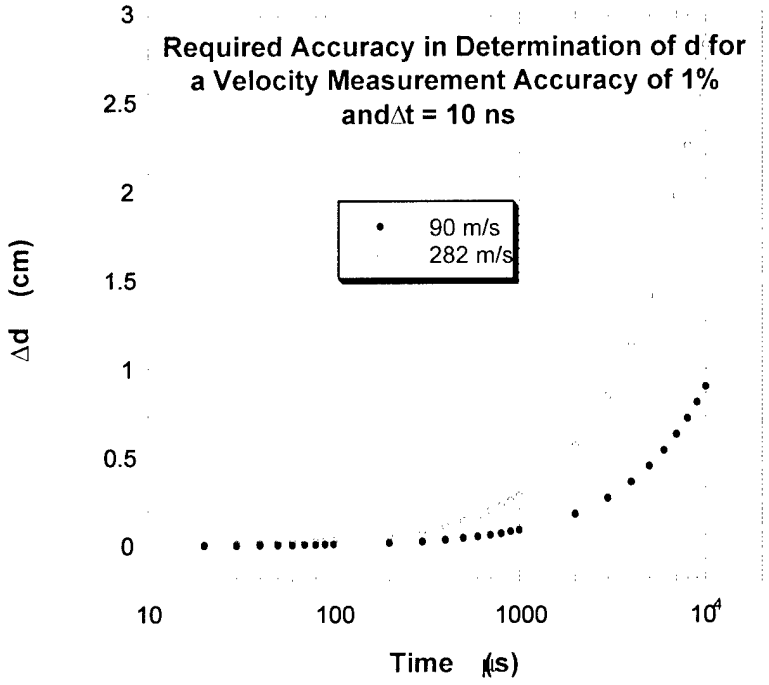

Figure 13. Required accuracy in determination of the displacement, *d*, for a velocity measurement accuracy of 1%.

For the conditions stated, a measurement time of $t \geq 10$ ms implies that the required accuracy in measuring the position d is greater than or equal to the spot size of the diffusionally-broadened marker volume. For example, a measurement time of $t > 10$ ms and $\Delta t = 10$ ns, a displacement accuracy of $\Delta d \leq$ *FWHM(t)* will yield a velocity accuracy of $\Delta v/v = 0.01$. As evidenced by our results for OTV, knowledge of the displaced line position is well within this boundary, and therefore the 1% accuracy in velocity measurement requirement is certainly within the specifications for the OTV prototype core.

CONCLUSIONS

In this Phase II effort we developed a prototype core of an OTV instrument for measuring the structure of velocity flow fields for ground testing of aircraft turbine engines. The approach demonstrated an entirely new molecular flow tagging technique suitable for a wide variety of unseeded flows and application to

inlet flows of aircraft turbine engines. Since OTV is immune to the effects of water vapor, the method is particularly well-suited to the flows of varying humidity at AEDC.

In Phase II, we redesigned the Phase I breadboard concept to produce a prototype core appropriate for large-scale facilities. The broadband excimer was replaced with two tunable, narrowband excimer lasers. The new lasers allowed enhanced measurements at higher temporal, spatial, and spectral resolution over larger areas. One of these lasers has been delivered to AEDC. The second laser is currently being put to use in the Vanderbilt laboratory in an investigation into high temperature molecular flow tagging applications.

In Phase II we theoretically and experimentally addressed the operating envelope for applying the OTV method. The dominating limits on the technique are temperature and time. The upper limit on temperature is approximately 600 K. At this temperature, the ozone marker begins to thermally decompose and react with other constituents in the flow. The limit imposed by time is a function of molecular diffusion. A reasonable upper limit on time delay between the write and read laser pulses is on the order of a ms.

In terms of future research and development, new software algorithms promise to enhance spatial resolution by accurately interpolating between OTV markers. These developments may minimize the need for generating a denser grid matrix.

At present, the cost of the two excimer laser systems prohibit broad commercial acceptance; however, this situation could change as more powerful, less expensive UV laser sources become available.

REFERENCES

1 Pitz, R.W., Brown III, T.M., and DeBarber P.A., "Method and apparatus for determining the velocity of an air flow," U.S. Patent # 5,708,495 issued January 13, 1998.

2 Kohl, R.H., "Development of Local Nonintrusive Measurements of Inlet and Exhaust Flows for the Ground Testing of Air-breathing Engines," AIAA Paper No. 92-3899, AIAA 17th Aerospace Ground Testing Conference, Nashville, TN, July 6-8, 1992.

3 Drain L E, 1980, The Laser Doppler Technique (New York: Wiley).

4 Adrian, R. J., 1991 "Particle imaging techniques for experimental fluid mechanics" *Annu. Rev. Fluid Mech.* Vol. 23, pp. 261-304.

5 Measures, R M., 1968, "Selective excitation spectroscopy and some possible applications" *J. Appl. Phys* Vol. 39, pp. 5232-5245.

6 Zimmermann, M., and Miles, R.B., 1980, "Hypersonic-helium-flow-field measurements with the resonant Doppler velocimeter" *Appl. Phys. Lett.* Vol. 37 pp. 885-887.

7 McDaniel J.C., Hiller, B., and Hanson, R.K., 1983, "Simultaneous multiple-point velocity measurements using laser-induced iodine fluorescence" *Opt. Lett.* Vol. 8 pp. 51-53.

8 Paul P.H., Lee, M.P., and Hanson, R.K., 1989, "Molecular Velocity Imaging of Supersonic Flows Using Pulsed Planar Laser-Induced Fluorescence of NO" *Opt. Lett.* Vol. 14, pp. 417-419.

9 Seasholtz R.G, Zupanc, F.J., and Schneider, S.J., 1992, "Spectrally resolved Rayleigh scattering diagnostic for hydrogen-oxygen rocket plume studies" *J. Prop. Power* Vol. 8, pp. 935-942.

10 Forkey, J.N., Finkelstein, N.D., Lempert, W.R., and Miles, R.B., 1996, "Demonstration and characterization of filtered Rayleigh scattering for planar velocity measurements" *AIAA J.* Vol. 34 pp. 442-448.

11 Hiller, B., Booman, R.A., Hassa, C., and Hanson, R.K., 1984, "Velocity visualization in gas flows using laser-induced phosphorescence of biacetyl" *Rev. Sci. Instrum.* Vol. 55 pp. 1964-1967.

12 Stier, B., and Koochesfahani, M.M., 1999, "Molecular tagging velocimetry (MTV) measurements in gas phase flows" *Exp. in Fluids* Vol. 26, pp. 297-304.

13 Orlemann, C., Schulz, C., and Wolfrum, J., 1999, "N_O-flow tagging by photodissociation of NO_2. A new approach for measuring small-scale flow structures" *Chem. Phys. Lett.* Vol. 307 pp. 15-20.

14 Boedecker, L.R., 1989, "Velocity measurement by $H2_0$ Photolysis and laser-induced fluorescence of OH" *Opt. Lett.* Vol. 14, pp. 473-475.

15 Miles, R.B., and Lempert, W.R., 1997, "Quantitative flow visualization in unseeded flows" *Annu. Rev. Fluid Mech.* Vol. 29 pp. 285-326.

16 Freisinger, B., Kogelschatz, U., Schafer, J.H., Uhlenbusch, J., and Viol, W., *Appl. Phys. B* Vol. 49, 121 (1989).

17 Laufer, G., McKenzie, R.L., and Fletcher, D.G., *Appl. Opt.* Vol. 29, p. 4873 (1990).

18 Park, H. and Slanger, T.G., *J. Chem. Phys.* Vol. 100, p. 287 (1994).

19 Lutz, A E, Kee, R.J., and Miller, J.A., 1988 "SENKIN: A Fortran Program for Predicting Homogeneous Gas Phase Chemical Kinetics with Sensitivity Analysis" (Sandia National Laboratories: Report SAND87-8248, Livermore, CA)

20 Wehrmeyer, J.A., Ribarovm L.A., Oguss, D.A., Batliwala, F, Pitz, R.W., and DeBarber, P.A., "Flow tagging velocimetry for low and high temperature flowfields" AIAA 37th Aerospace Sciences Meeting Paper 99-0646, January 1999.

21 Lee, M., 1991, "Temperature measurements in gases using planar laser-induced fluorescence imaging of NO and O_2" Ph.D. Thesis (HTGL Report T-282) Mechanical Engineering Department, Stanford University, USA.

22 Finlayson-Pitts, B.J., and Pitts, J.R., Jr., 1986, "Atmospheric Chemistry: Fundamentals and Experimental Techniques" (New York: Wiley-Interscience).

23 Bevington, P.R., and Robinson, D.K., "Data Reduction and Error Analysis for the Physical Sciences," (McGraw-Hill, Inc., NY, 1992).

24 Conversations with AEDC personnel, August 28, 1997.